

Tip-enhanced near-field Raman spectroscopy with a scanning tunneling microscope and side-illumination optics

K. J. Yi, X. N. He, Y. S. Zhou, W. Xiong, and Y. F. Lu

Citation: *Rev. Sci. Instrum.* **79**, 073706 (2008); doi: 10.1063/1.2956977

View online: <http://dx.doi.org/10.1063/1.2956977>

View Table of Contents: <http://rsi.aip.org/resource/1/RSINAK/v79/i7>

Published by the [AIP Publishing LLC](#).

Additional information on *Rev. Sci. Instrum.*

Journal Homepage: <http://rsi.aip.org>

Journal Information: http://rsi.aip.org/about/about_the_journal

Top downloads: http://rsi.aip.org/features/most_downloaded

Information for Authors: <http://rsi.aip.org/authors>



New, Easy-to-Mount
FLIR A6700sc Camera

When you need Science-Grade IR in Tight Spaces

FLIR

Get Datasheet 

The advertisement features a black FLIR A6700sc camera mounted on a yellow and orange printed circuit board. The background is a dark blue grid pattern. The FLIR logo is visible on the camera and in the bottom right corner.

Tip-enhanced near-field Raman spectroscopy with a scanning tunneling microscope and side-illumination optics

K. J. Yi, X. N. He, Y. S. Zhou, W. Xiong, and Y. F. Lu^{a)}

Department of Electrical Engineering, University of Nebraska-Lincoln, Lincoln, Nebraska 68588-0511, USA

(Received 2 May 2008; accepted 18 June 2008; published online 16 July 2008)

Conventional Raman spectroscopy (RS) suffers from low spatial resolution and low detection sensitivity due to the optical diffraction limit and small interaction cross sections. It has been reported that a highly localized and significantly enhanced electromagnetic field could be generated in the proximity of a metallic tip illuminated by a laser beam. In this study, a tip-enhanced RS system was developed to both improve the resolution and enhance the detection sensitivity using the tip-enhanced near-field effects. This instrument, by combining RS with a scanning tunneling microscope and side-illumination optics, demonstrated significant enhancement on both optical sensitivity and spatial resolution using either silver (Ag)-coated tungsten (W) tips or gold (Au) tips. The sensitivity improvement was verified by observing the enhancement effects on silicon (Si) substrates. Lateral resolution was verified to be below 100 nm by mapping Ag nanostructures. By deploying the depolarization technique, an apparent enhancement of 175% on Si substrates was achieved. Furthermore, the developed instrument features fast and reliable optical alignment, versatile sample adaptability, and effective suppression of far-field signals. © 2008 American Institute of Physics. [DOI: 10.1063/1.2956977]

I. INTRODUCTION

Raman spectroscopy (RS), as a powerful optical spectroscopic technique, has been widely applied to a variety of fields such as chemistry, physics, material science, biology, space exploration, and semiconductor industry.¹ The applications attribute to the unique capability of identifying structures and chemical bonding through characterizing molecular vibrations of the constituent atoms or ions. However, conventional RS faces two challenges: (1) the inherited notoriously weak scattering sensitivity resulting from small interaction cross sections (10^{-29} cm²/molecule) and (2) low spatial resolutions (1 μ m) dictated by the optical diffraction limit.² In line with the challenges, different schemes have been proposed. Represented by near-field RS (NFRS),³ surface-enhanced RS (SERS),^{1,3-6} and tip-enhanced RS (TERS),⁷⁻⁹ these schemes are based upon one or more mechanisms of electromagnetic enhancement, chemical enhancement, and near-field effects. NFRS, referring to aperture RS, has demonstrated a spatial resolution of 100 nm by employing an aperture with a diameter of 100 nm on a tapered fiber tip or micropipette. Further resolution improvement is nearly impossible because of an extremely low optical throughput of the optical fiber with diameters below 100 nm. SERS employs rough metallic surfaces (Ag, Au, etc.) formed by grains, fractals, clusters, and nanoparticles to achieve presently the strongest Raman enhancement with an enhancement factor of 10^{14} .¹⁰ This impressive enhancement is mostly explained by local surface plasmons (LSPs) induced by rough metallic surfaces. LSPs are charge-density oscillations confined to metallic nanoparticles or nanostructures.

Excitation of LSPs by an optical field with a wavelength, at which the resonance occurs, results in strong light scattering, the appearance of intense absorption bands due to surface plasmons (SPs), and an enhancement of the local electromagnetic fields.¹¹ This technique allows the sensing of an individual molecule.¹⁰ However, the morphologies of the metal surfaces, which ultimately determine the SERS effect, are uncontrollable, and hence severely limit the quantitative analyses.

TERS, on the other hand, makes use of a metallic tip to induce LSPs. Investigators found that a highly localized and significantly enhanced electromagnetic field can be generated in the proximity of the metallic tip irradiated by a laser beam.^{12,13} It is suggested that in addition to LSPs, lightning-rod effect may also contribute to the enhancement due to the geometric singularity.⁸ One can take advantages of the localized field to improve both the lateral resolution and detection sensitivity because the enhancement only occurs in a nanometer range dictated by the geometry of the tip apex. However, this evanescent field degrades rapidly along the light propagation direction. To make use of the local field, one must precisely control the tip-surface distance at a nanometer or angstrom level. Practically, the precise distance control can be realized by a scanning probe microscope (SPM) which uses either atomic force for atomic force microscope (AFM) or tunneling current for scanning tunneling microscope (STM) as the control variables. Both AFM and STM can provide atomic-resolution images by scanning a tip across sample surfaces and monitoring either the atomic force or tunneling current. RS in conjunction with SPM may provide a new insight into understanding the morphology, electronic, thermal, chemical, mechanical, and optical properties of nanoscale materials and devices in a correlated fashion, eliminating sample contamination during transportation

^{a)} Author to whom correspondence should be addressed. Tel.: 402-472-8323. Electronic mail: ylu2@unl.edu.

among different instruments. Recently, both AFM-combined RS (RAFM) and STM-combined RS (RSTM) have been reported.^{12,14–21} For RAFM, an AFM works in the contact mode with a Au or Ag coated Si tip as the light scatter. While for RSTM, a STM runs in the constant-current mode with the tip above the sample surface in a tunneling range. Up until now, most TERS-related reports on how to build TERS systems are focused on RAFM,^{12,14,15,17–21} while only a few reports have systematic description of building RSTMs. One typical example of RSTM is that a high-resolution RSTM system was built using a parabolic mirror with a high numerical aperture (NA) to study thin layers and nanostructures in an ultrahigh vacuum.¹⁶ However, the presence of the parabolic mirror not only increases the system complexity but also adds difficulties to optical alignment. So far, there is no report on how to perform fast and reliable optical alignment although it is a critical prerequisite to realize Raman enhancement. Several instrument suppliers such as Tokyo Instruments, Renishaw, Witec, JPK instruments, and Jobin-Yvon are making strong efforts on developing a versatile and dynamic TERS system.

RSTM offers many advantages over RAFM, such as (1) better lateral resolution by precisely controlling the tip-sample gap distance, (2) gap mode resonances of the tip-sample configuration, and (3) feasibility of electronic property characterization in conjunction with RS chemical identification. TERS systems can be categorized in bottom or side illumination.^{20,22} For transparent samples, the bottom illumination is more popular due to high optical throughput and convenient optical alignment. For opaque samples, however, the side illumination is the only approach although it suffers from inconvenient optical alignment and strong background signals.

In this study, we developed a RSTM system using the side-illumination optics, with the capability of receiving both far-field and near-field Raman signals. By appropriate optical design and three specific alignment steps, fast and reliable optical alignment is achieved. Meanwhile, the far-field signals have been significantly suppressed by depolarization. As a result, a higher contrast ratio has been achieved.^{15,23} The high contrast ratio allows clear Raman mapping of nanostructures or residual stress distribution in devices. The system can be converted to a RAFM system by replacing the STM nose cone with an AFM one. The flexible transformation from RSTM to RAFM allows nanoscale Raman spectroscopy for both conductive and insulating samples.

Tip material and geometries are important factors for the Raman enhancement.^{13,24,25} This study investigated and compared the preparation and TERS performance of both Au tips and Ag-coated W tips. Ag nanostructures fabricated on Si substrates by the nanosphere lithography (NSL) technique were used for system evaluation because the LSPs induced by nanoscale dipoles are promising to further enhance the local optical field in addition to TERS.

II. EXPERIMENTAL

A. System description

The schematic of the developed TERS system is depicted in Fig. 1. The system consists of an optical path, a

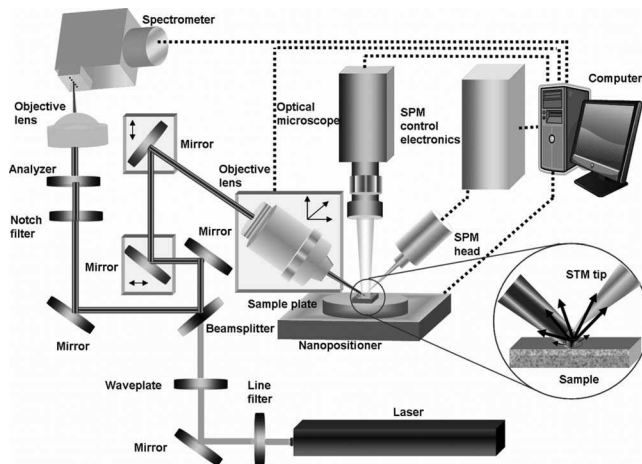


FIG. 1. Schematic of the RSTM system using side-illumination optics. Dashed lines indicate electronic connections.

spectral acquisition module [spectrograph and charge coupled device (CCD) camera], a STM module, a motorized stage module, an optical microscope, and a computer. The optical path is used to deliver the excitation laser beam onto sample surfaces as well as collect the Raman signals from the surfaces. The spectral acquisition module is used to collect the scattered signals and convert the optical signals into electronic data. Tip-surface distance is controlled by the STM. The motorized stage module is used to position the samples. The optical microscope equipped with a CCD camera plays the roles of locating the regions of interest and monitoring the optical alignment. The computer is used to control the STM as well as acquire, process, and visualize the Raman signals.

The instrument can accommodate both AFM and STM functionalities to combine with the Raman spectrometer. The three-dimensional optical path can precisely and reliably align the laser beam on the tip. A SPM system (Agilent, SPM 5500) is used as a platform to build the TERS system. The tip is mounted on a piezoelectric transducer that has a stroke of 100 μm and a closed-loop control. In addition, a two-axis nanopositioner (Mad City Laboratories, nano-H100) is placed beneath the sample holder. The nanopositioner is used for mapping sample surfaces. The software used for mapping is developed using the LABVIEW™ programming platform together with the instrumental drivers provided by the hardware suppliers.

In Fig. 1, a laser beam from an argon laser (Coherent, Innova 300) passes through a line filter (Newport) that only allows the wavelength of 514.5 nm to pass through. Before reaching a beam splitter (Newport), the beam is reflected by a mirror, and its polarization is varied by a half-wave plate (CVI). The transmitted beam is then reflected by three mirrors before being focused on a sample surface by an objective lens (Olympus, LWD50X, NA=0.45, WD=15 mm). Afterwards, the STM tip approaches the sample surface with the tip-surface distance in the tunneling range of 1 nm. The status of the tip, the laser beam, and the substrate surface are monitored by the optical microscope. The position of the objective lens is controlled by a motorized XYZ stage with a resolution of 3 μm , indicated by the box outside the objec-

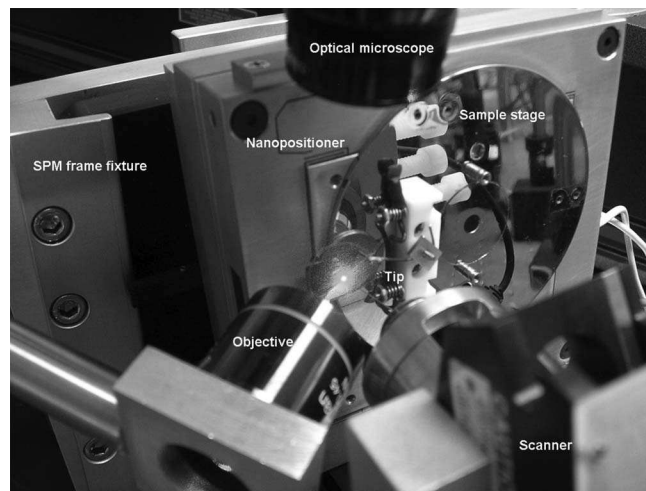


FIG. 2. Experimental setup of the RSTM system.

tive lens shown in Fig. 1. With a successful optical alignment, near-field Raman scattering signals are collected by the objective lens and reflected by the mirrors. After passing through a notch filter (Kaiser, SuperNotch®, OD=4.0) and an analyzer (Newport), the beam with Raman signals is focused by a lens (CVI) into the slit of the spectrograph (Acton Research, Spectro-2300i). A back-illuminated CCD camera (Princeton Instruments, PIXIS-400B) with a high quantum efficiency (>90% at 514.5 nm) is used to acquire the Raman spectra. The spectra are then analyzed, processed, and visualized by the computer.

To perform Raman mapping, a sample is placed on the nanopositioner which has a lateral resolution of 0.4 nm. Figure 2 shows a picture for the practical experimental setup. It can be seen that both the STM system and the motorized sample module are placed on a fixture frame.

B. SPM electronics

A SPM from Agilent Technologies was selected for building the TERS system due to its open architecture. This SPM has a sufficient space to incorporate other modules. The SPM system accommodates different operation modes of contact AFM, noncontact AFM, current sensing AFM, STM, and scanning tunneling spectroscopy (STS). The SPM system is composed of an optical microscope, a motor, a four-segment *PIV* laser diode, an environment chamber, a main frame, and three scanners including one STM-only scanner with a 1 μm scanning range (9501A), one STM-AFM scanner with a 10 μm scanning range (9520A), and one STM-AFM scanner with a 100 μm scanning range (9524A).

C. Optical alignment

To obtain the TERS, precise alignment of the focused laser beam with respect to the tip is essential. The beam center should be aligned in between the tip-surface gap, with the challenge that the micron-sized laser beam is required to be aligned with the nanoscale tip apex. Three steps of coarse, intermediate, and precise alignments are used to address this challenge. More specifically, the laser beam is

aligned to the tip with a millimeter-range accuracy in the coarse alignment, a micrometer-range accuracy in the intermediate alignment, and a nanometer-range accuracy in the precise alignment.

As shown in Fig. 1, two mirrors (in boxes), one objective lens (in a box), and one tip, all movable, are the key components to perform the optical alignment. Both mirrors, mounted on two orthogonally arranged translation stages, are used to perform the coarse alignment. The objective lens, mounted on the motorized *XYZ* stage, is used for the intermediate alignment. The precise alignment is implemented by the piezoelectric transducer mounted on the STM scanner. The tip position and sample surface are both monitored by the optical microscope. Before the coarse alignment, the objective lens is moved away from the optical path. The laser beam is positioned in a targeted region completely covering the tip apex. The objective lens then moves back and gradually approaches the sample surface. When the optical path is well aligned, the focused laser beam is always along the desired propagation direction. At this stage, the position of the focused beam should be near the tip position. Subsequently, by moving the objective lens in the intermediate alignment, the focused beam is brought to the tip position with an accuracy of 50 μm . Finally, the tip is brought back and moves in a range of 100 μm with a resolution of 0.4 nm. Since the beam is within a range of 50 μm from the tip position, the laser beam eventually meets with the tip at a certain position.

D. Tip and substrate fabrication

Two types of tips can be employed: Ag/Au-coated W tips and Au tips.^{24–27} Enhancement from Ag tips is slightly stronger than that from Au tips. However, due to oxidation when exposed in air, Ag tips may lose enhancement effects after 2 or 3 days. Compared to the fabrication of Ag-coated W tips in which an additional sputtering process is needed, the preparation of Au tips is simpler because only the etching process is necessary. However, Au tips are too soft and easily deformed when they scan on or retract from sample surfaces. In contrast, the W tips are harder and barely deformed. In this study, both Ag-coated W tips and Au tips were prepared to evaluate the TERS performance.

The W and Au tips were fabricated by a direct current electrochemical etching apparatus. Etching voltage, etching time, configuration of cathode, and solution are different for fabricating each type. To fabricate a W tip, a W wire (Aldrich) of 0.25 mm diameter was immersed in a solution with a mixture of concentrated HClO_4 and pure methanol (1:4) at an anodic voltage of 1.8 V. The etching time was around 9 min. The W tip was then placed into a vacuum chamber of a sputtering system to coat with a Ag layer of 40 nm thick. To fabricate a Au tip, a Au wire (Aldrich) of 0.25 mm diameter was immersed in a solution prepared using analytical grade fuming hydrochloric acid and ethanol (Merck). To achieve a smooth surface, the anode was made in a ring shape. A bias voltage of 2.4 V was then applied between the ring and the Au tip for a time period of around 5 min.

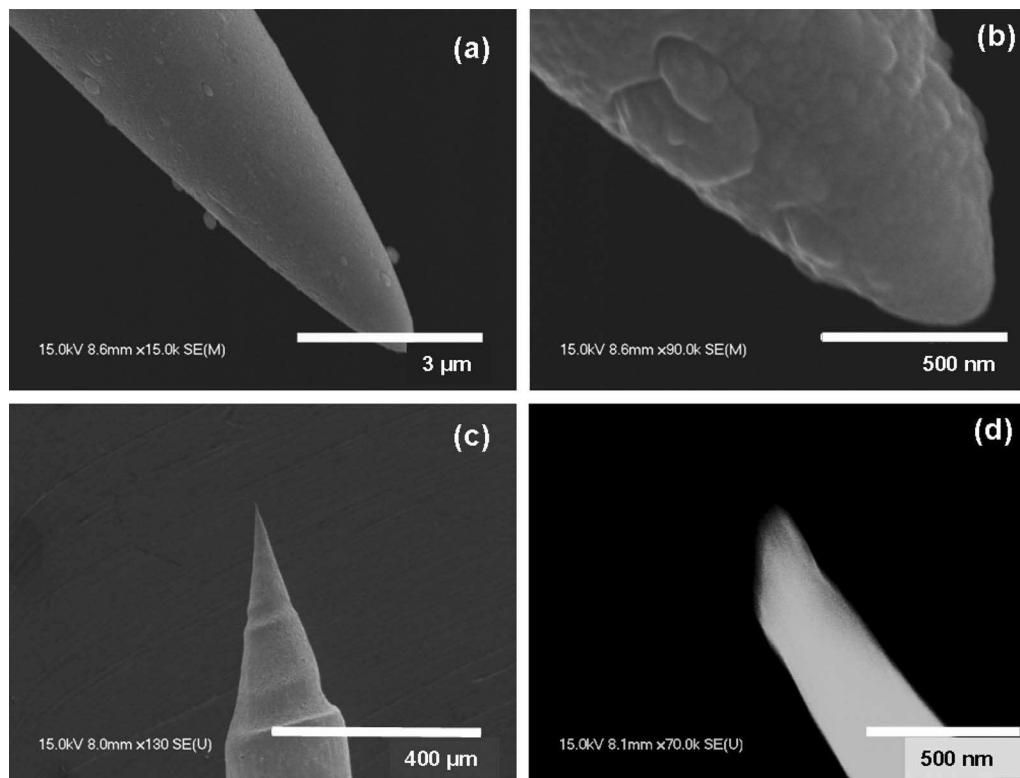


FIG. 3. SEM micrographs of (a) normal view, (b) zoomed view of a Ag-coated W tip, as well as (c) normal view and (d) zoomed view of a Au tip.

P-type Si (110) substrates (Virginia Semiconductor) with a resistivity of 0.02–0.09 Ω cm were cleaned in an ultrasonic cleaner with acetone and alcohol solutions for 10 min each, followed by a passivation process in 5% HF solution for 5 min. The substrates were then dried with a nitrogen gas. Ag nanostructures were fabricated on the Si substrate by the NSL process followed by a sputtering process. Silica microparticles with a diameter of 800 nm were used as masks for sputtering Ag on the substrates. After the lift-off process, triangle-shaped Ag nanostructures were formed on the substrate surfaces. The side length of the nanostructures was 200 nm with a tip-to-tip distance of around 100 nm.

III. RESULTS AND DISCUSSION

A. The Ag-coated W tip and Au tip

The micrographs of the Ag-coated W tip and tip apex are shown in Figs. 3(a) and 3(b), respectively. A smooth Ag layer was deposited on the tip surface. It was reported that a smaller tip apex radius can lead to a stronger enhancement.²⁴ In this study, the radius of the tip apexes was around 50 nm. In Fig. 3(a), Ag grains with sizes of around 10 nm are found in the tip apex region, which also possibly contribute to the Raman enhancement since the grain structures are the major mechanism to achieve substantial enhancement in SERS. The micrographs of the Au tip and tip apex are shown Figs. 3(c) and 3(d).

B. Simulation of local optical fields

Simulation of locally enhanced optical fields beneath the tip apexes provides insight into the mechanisms behind the

enhancement as well as information on how to optimize the enhancement by coordinating relevant factors such as tip material, tip geometry, excitation wavelength, incident angle, and polarization direction.²⁸ Different approaches, e.g., *T*-matrix approach, Mie's theory, finite element analysis, and finite difference time domain (FDTD), have been used to perform the simulation.²⁷ In this study, the FDTD algorithm in conjunction with the Lorentz–Drude model under the perfectly matched layer boundary conditions was used to simulate the optical fields. This model has taken the Si substrate into consideration.

The physical model is depicted in Fig. 4(a). One conical Ag tip with a diameter of 50 nm is placed 1 nm above a flat Si surface and illuminated by a Gaussian-shaped continuous-wave laser with a wavelength of 514.5 nm propagating along the *k* direction. The incident angle is 65° with respect to the tip axis (*X* axis). The beam is polarized in parallel with the tip for optimal coupling. The magnitude of the electric field of the beam is assumed to be 1 V/m. The uniform mesh step for each axis is 0.5 nm. Figure 4(b) shows the electric field distribution in a two-dimensional view. It can be observed that the electric field as high as 600 times is locally enhanced in the space between the tip apex and the substrate surface in a region of 14 nm, indicating that a spatial resolution of 14 nm could be achieved.

C. Optical alignment

Three steps have been used for fast and reliable optical alignment. Figures 5(a)–5(c) are the images of the Ag-coated W tip and laser beam under different conditions as monitored by the optical microscope. Figure 5(a) shows that

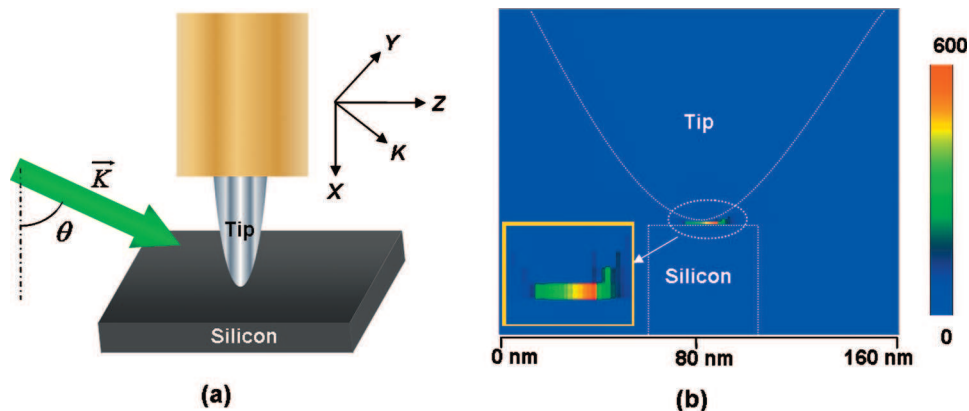


FIG. 4. (Color) (a) Physical model to simulate the optical field in the proximity of a Ag-coated W tip. (b) Optical field distribution in the proximity of a Ag-coated tip illuminated by a 514.5 nm laser beam. The inset is a zoomed view of the optical field distribution.

the tip was away from the substrate, in which only far-field Raman signals can be obtained. A mirrored image of the tip can be observed due to the reflection from the substrate surface. Figure 5(b) shows the scattered light at the tip apex when the laser beam was focused on the tip. A mirrored diffraction image is present, indicating that the laser beam was not exactly positioned in the tip-surface gap but slightly toward the tip. The focused laser beam was thus partially blocked by the tip, so that the total Raman intensity was reduced. Figure 5(c) shows the diffraction pattern in an ideal alignment where the enhanced Raman intensity can be observed. The strong interference patterns around the tip apex are generally used to identify the optimal alignment between the tip and the sample surface. Likewise, Fig. 5(d) shows the diffraction pattern from a Au tip in good optical alignment.

D. Raman spectra of the Si substrates

Contrast ratio, defined as the ratio of near-field to far-field Raman intensity, is used to evaluate the extent of the enhancement. The far-field intensity is obtained when the laser beam is far away from the tip, ensuring no tip-beam

interaction exists. Subtracting the far-field intensity from the total intensity equals to the near-field intensity when the laser beam is well aligned with the tip to achieve strong near-field effects. It is reported that the contrast ratio of the crystalline Si at 520 cm^{-1} is around 50% by Ag-coated W tips or Au tips.^{19,26} Figure 6(a) shows the Raman spectra of the Si substrate with the Ag-coated W tip under different conditions. The total intensity in a well aligned case, the far-field intensity, and the total intensity in a misaligned case in which the laser beam was partially blocked are indicated by Raman spectra 1, 2, and 3, respectively. In a well aligned case, a contrast ratio of 52% can be observed (spectrum 1). Whereas when the beam was blocked by the tip, the intensity was significantly reduced due to the “shadowing effects” (spectrum 3).¹⁹ Figure 6(b) shows the Raman spectra of the Si substrate with a Au tip. A contrast ratio of 47% was obtained.

E. Far-field suppression using the depolarization technique

To further improve the contrast ratio, several methods have been employed including tip material and geometry modification,²⁹ excitation wavelength selection or plasma resonance tuning,³⁰ optical system optimization, and use of excitation and scattering light polarization.³¹ The common rationale of these approaches is to increase the near-field intensity. Nevertheless, there is an alternative way to increase the contrast ratio by suppressing the far-field intensity. Raman scattering signals are generated from the interaction between a polarized incident laser beam and molecular vibrations. With different symmetry of the vibration mode, the scattered signal can be polarized either parallel or perpendicular to the polarization direction of the incident beam or both. For symmetric vibrations, the scattered light is almost completely polarized in the same direction as the incident field, and no depolarization can be observed. Whereas, the scattered light from asymmetric vibrations is polarized both parallel and perpendicularly to the incident beam. Since crystalline Si has a highly symmetric structure, the Raman scattering is strongly polarized. For example, the polarization of the incident beam can be locally changed around the vicinity of diamond nanoparticles.³² The sharp apexes of Ag

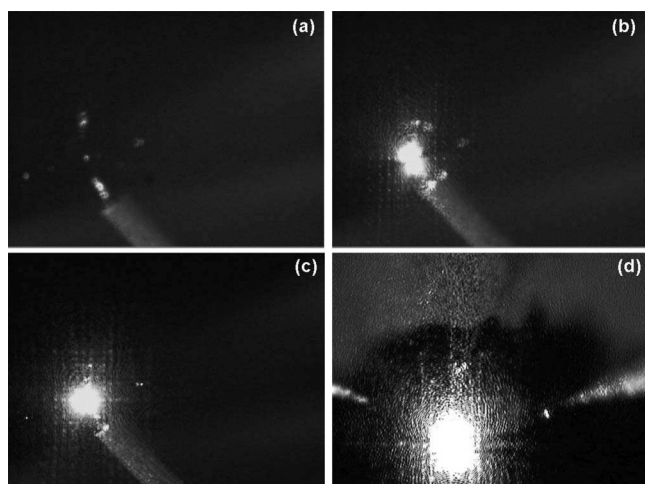


FIG. 5. Images captured in the optical alignment under the conditions of (a) beam away from the tip, (b) beam on the tip, and [(c) and (d)] tip in the center of the tip-surface gap (good alignment). (a)–(c) are for a Ag-coated W tip and (d) is for a Au tip.

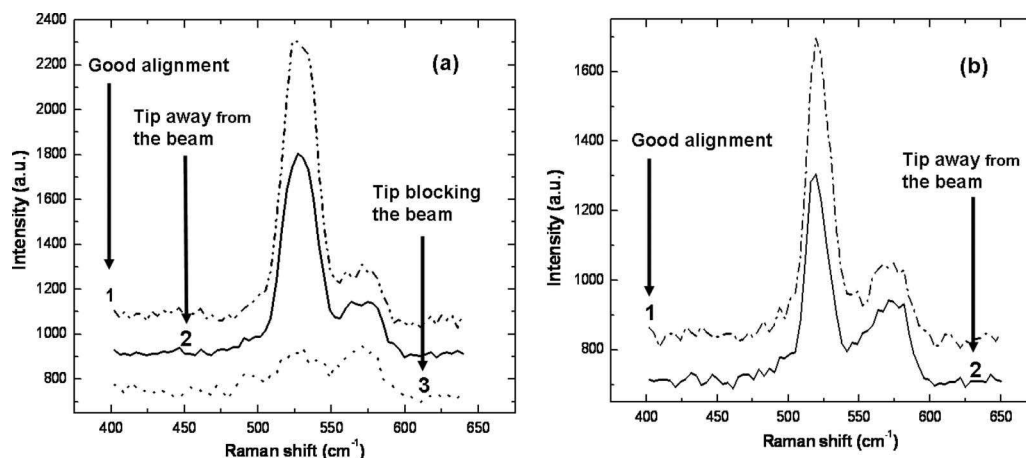


FIG. 6. Raman spectra of the Si substrate using (a) a Ag-coated W tip and (b) a Au tip. Spectra 1, 2, and 3 were taken in the cases of good alignment, laser beam away from the tip, and laser beam on the tip but not in the gap, respectively.

tips should be able to play the same role as that of the diamond particles. If an analyzer were oriented perpendicular to a polarizer, the far-field signals could be blocked by the analyzer since most scattered Raman signal has the same orientation as the polarizer. The tip interaction with the incident light changes the polarization, which leads to the depolarization such that there is partial depolarization of the incident beam in its vicinity. Recently, using depolarization technique to efficiently suppress the far-field signals has been reported.¹⁵ This depolarization technique was further optimized to successfully obtain Raman images with high contrast.¹⁹

In the experiments, the analyzer was kept perpendicular to the tip axis, while the polarizer was rotated at a step of 15° . Shown in Fig. 7 are the far-field intensity, near-field intensity, and contrast ratio as functions of the polarizer angle, which is defined as the polarization direction of the incident beam with respect to the sample surface. The far-field signals were collected when the tip was far away from the beam. The near-field signals were collected when the tip was well aligned with the beam. By changing the polarizer angle, different Raman intensities at the peak position of

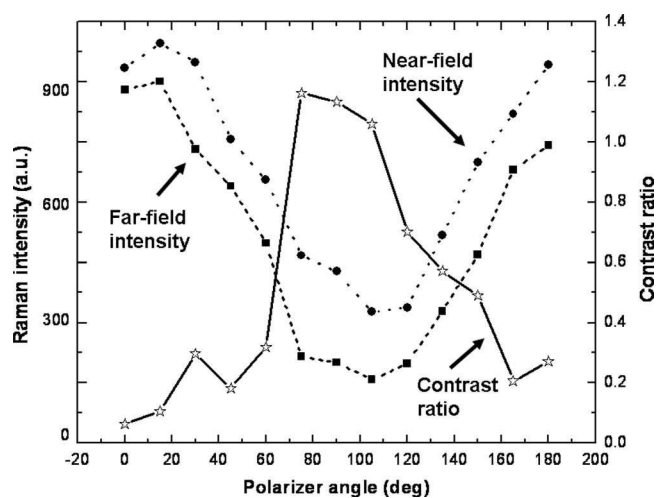


FIG. 7. Far-field intensity (squares), near-field intensity (diamonds), and contrast ratio (stars) as functions of the polarizer angle.

520 cm^{-1} were captured, and thus the contrast ratios were obtained. It can be clearly seen that a contrast ratio as high as 120% has been achieved when the polarizer angle is between 90° and 105° using the Ag-coated W tip. The Raman spectra of the Si substrate from the W tip are shown in Fig. 8(a) when the depolarization technique was employed. This enhancement is more than doubled with the depolarization. The Raman spectra of the Si substrate from a Au tip are shown in Fig. 8(b), with a contrast ratio of 175%. The results demonstrate that the depolarization technique is effective to improve the contrast ratio.

F. Raman mapping of Ag nanostructures

The spatial resolution of the TERS (RSTM) system was investigated by mapping the Ag nanostructures fabricated on Si substrates. Figure 9(a) shows the scanning electron microscopy (SEM) micrograph of the Ag nanostructures. They have triangle geometries with a side length of around 200 nm and a tip-to-tip distance of around 100 nm. Since the focused laser beam has a diameter of $3\text{--}5\ \mu\text{m}$, the normal RS cannot resolve the individual nanostructures. Without further efforts, 20 nanoscale triangles would be covered in the focused laser spot. The RSTM has the capability of distinguishing the nanostructures. The tip apex has a radius of around 30 nm, smaller than the size of each triangle. Consequently, the tip could be precisely positioned on one nanostructure. The near-field signals varied in different regions. When the tip was on the nanostructures, no obvious enhancement on Si spectrum was observed. When the tip was in the region between two tips of the triangles, the strongest enhancement was observed due to the strong LSPs induced by the particular arrangement. By scanning the STM tip in a range, a Raman image was obtained as illustrated in Fig. 9(b). The image in Fig. 9(b) corresponds to the area enclosed with the dashed lines in Fig. 9(a). It could be seen that the spatial resolution of the RSTM is well below 100 nm, much smaller than the optical diffraction limit.

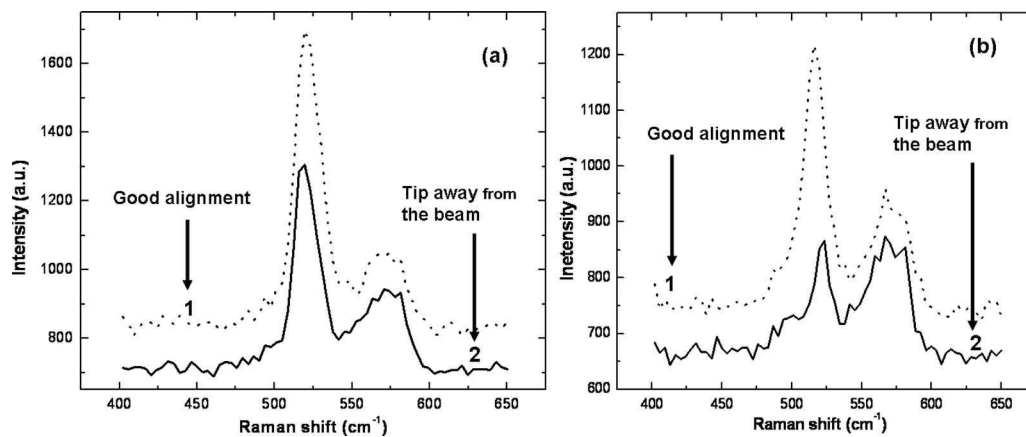


FIG. 8. Raman spectra of the Si substrate using (a) the Ag-coated W tip and (b) the Au tip with depolarization. Spectra were taken in the cases of good alignment and beam away from the tip, respectively.

IV. CONCLUSIONS

A TERS system, which consists of both a Raman spectrometer and a scanning tunneling microscope, was developed to improve both the spatial resolution and detection sensitivity. Using side-illumination optics, the TERS instrument can accommodate both opaque and transparent samples. The flexible optical design and alignment procedure provide a reliable and rapid alignment to match the focused laser beam with the STM tip. Both Ag-coated W tips and Au tips were fabricated and used in this study. The far-field signals have been efficiently suppressed by depolarization. A contrast ratio as high as 175% on the Si substrate was obtained using a Au tip. The spatial resolution of the instrument was proved to be below 100 nm by mapping Ag nanostructures on a Si substrate. Therefore, the developed RSTM system features fast and reliable optical alignment, versatile sample adaptability, and sufficient far-field signal suppression. The correlated characterization capability of the system provides a new approach to understanding the relationship among the morphology, electronic, thermal, chemical, mechanical, and optical properties of nanoscale materials and devices, while eliminating sample contaminations during transportation among different instruments. This instrument can be used for spectroscopic studies of a variety of optical phenomena such as light emission, fluorescence, one-photon and two-photon excitations for possible applications encompassing virus detection, cancer therapy, biochemical identification, single molecule sensing, nanoelectronic device analysis, optical trapping, and nanofabrication.

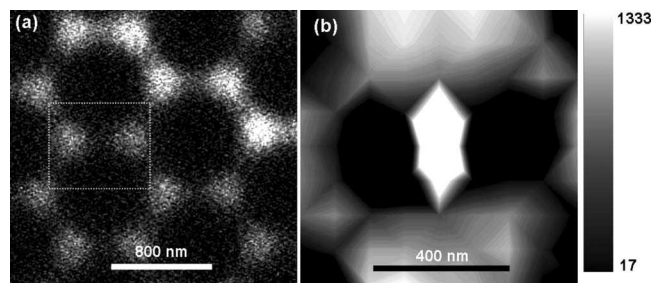


FIG. 9. (a) SEM micrograph and (b) Raman mapping image of Ag nanostructures fabricated on a Si substrate.

ACKNOWLEDGMENTS

The authors would like to thank Professor Natale J. Ianno in the Department of Electrical Engineering for providing the sputtering system to fabricate tips and nanostructures. The authors would also like to thank Dr. You Zhou at the Beadle Center of the Biology Department for the assistance of characterizing the tips and nanostructures using the SEM. The authors would like to acknowledge Mr. Mike Jensen at the Instrument Shop for his efforts in design and fabrication of the fixtures. This work was financially supported by the National Science Foundation (Nos. ECCS 0619553 and ECCS 0652905) and the Nebraska Research Initiative.

- ¹M. Moskovits, *J. Raman Spectrosc.* **36**, 485 (2005).
- ²N. Hayazawa, Y. Inouye, Z. Sekkat, and S. Kawata, *Opt. Commun.* **183**, 333 (2000).
- ³E. J. Ayars and H. D. Hallen, *Appl. Phys. Lett.* **76**, 3911 (2000).
- ⁴E. C. Le Ru, E. Blackie, M. Meyer, and P. G. Etchegoin, *J. Phys. Chem. C* **111**, 13794 (2007).
- ⁵B. Pettinger, G. Picardi, R. Schuster, and G. Ertl, *Single Mol.* **3**, 285 (2002).
- ⁶A. Otto, I. Mrozek, H. Grabhorn, and W. Akemann, *J. Phys.: Condens. Matter* **4**, 1143 (1992).
- ⁷H. Watanabe, Y. Ishida, N. Hayazawa, Y. Inouye, and S. Kawata, *Phys. Rev. B* **69**, 155418 (2004).
- ⁸A. Hartschuh, M. R. Beversluis, A. Bouhelier, and L. Novotny, *Philos. Trans. R. Soc. London, Ser. A* **362**, 807 (2004).
- ⁹D. Richards, R. G. Milner, F. Huang, and F. Festy, *J. Raman Spectrosc.* **34**, 663 (2003).
- ¹⁰S. M. Nie and S. R. Emory, Abstr. Pap. - Am. Chem. Soc. **213**, 177 (1997).
- ¹¹A. J. Haes, W. P. Hall, and R. P. Van Duyne, *Laser Focus World* **41**, 105 (2005).
- ¹²A. Barbara, T. Lopez-Rios, and P. Quemerais, *Rev. Sci. Instrum.* **76**, 023704 (2005).
- ¹³N. Hayazawa, Y. Inouye, Z. Sekkat, and S. Kawata, *Chem. Phys. Lett.* **335**, 369 (2001).
- ¹⁴C. Vannier, B. S. Yeo, J. Melanson, and R. Zenobi, *Rev. Sci. Instrum.* **77**, 023104 (2006).
- ¹⁵A. Tarun, N. Hayazawa, M. Motohashi, and S. Kawata, *Rev. Sci. Instrum.* **79**, 013706 (2008).
- ¹⁶J. Steidtner and B. Pettinger, *Rev. Sci. Instrum.* **78**, 103104 (2007).
- ¹⁷Y. Saito, M. Motohashi, N. Hayazawa, M. Iyoki, and S. Kawata, *Appl. Phys. Lett.* **88**, 143109 (2006).
- ¹⁸L. T. Nieman, G. M. Krampert, and R. E. Martinez, *Rev. Sci. Instrum.* **72**, 1691 (2001).
- ¹⁹N. Lee, R. D. Hartschuh, D. Mehtani, A. Kisliuk, J. F. Maguire, M. Green,

- M. D. Foster, and A. P. Sokolov, *J. Raman Spectrosc.* **38**, 789 (2007).
- ²⁰N. Hayazawa, A. Tarun, Y. Inouye, and S. Kawata, *J. Appl. Phys.* **92**, 6983 (2002).
- ²¹N. Hayazawa, Y. Inouye, Z. Sekkat, and S. Kawata, *J. Chem. Phys.* **117**, 1296 (2002).
- ²²A. Hartschuh, E. J. Sanchez, X. S. Xie, and L. Novotny, *Phys. Rev. Lett.* **90**, 095503 (2003).
- ²³M. Motohashi, N. Hayazawa, A. Tarun, and S. Kawata, *J. Appl. Phys.* **103**, 034309 (2008).
- ²⁴B. Ren, G. Picardi, and B. Pettinger, *Rev. Sci. Instrum.* **75**, 837 (2004).
- ²⁵L. Billot, L. Berguiga, M. L. de la Chapelle, Y. Gilbert, and R. Bachelot, *Eur. Phys. J.: Appl. Phys.* **31**, 139 (2005).
- ²⁶W. X. Sun and Z. X. Shen, *Ultramicroscopy* **94**, 237 (2003).
- ²⁷W. X. Sun and Z. X. Shen, *J. Opt. Soc. Am. A* **20**, 2254 (2003).
- ²⁸K. J. Yi, H. Wang, Y. F. Lu, and Z. Y. Yang, *J. Appl. Phys.* **101**, 063528 (2007).
- ²⁹E. J. Sanchez, J. T. Krug, and X. S. Xie, *Rev. Sci. Instrum.* **73**, 3901 (2002).
- ³⁰P. Nordlander and F. Le, *Appl. Phys. B: Lasers Opt.* **84**, 35 (2006).
- ³¹N. Hayazawa, Y. Saito, and S. Kawata, *Appl. Phys. Lett.* **85**, 6239 (2004).
- ³²V. Poborchii, T. Tada, and T. Kanayama, *Jpn. J. Appl. Phys., Part 2* **44**, L202 (2005).